

# **Chitosan Metal Oxides Based Nanocomposites for Biosensing Application**

A DISSERTATION

SUBMITTED IN THE PARTIAL FULFILLMENT OF THE  
REQUIREMENT FOR THE AWARD OF THE DEGREE OF

MASTER OF TECHNOLOGY

in

**POLYMER TECHNOLOGY**

Submitted by

**VAIBHAV BUDHIRAJA  
2K16/PTE/07**

Under the supervision of

Dr. CHANDRA MOULI PANDEY

Dr. SAURABH MEHTA



DEPARTMENT OF APPLIED CHEMISTRY  
DELHI TECHNOLOGICAL UNIVERSITY  
Shahbad Daulatpur, Main Bawana Road  
Delhi-110042

DELHI TECHNOLOGICAL UNIVERSITY  
(Formerly Delhi College of Engineering  
Bawana Road, Delhi-110042

**CANDIDATE'S DECLARATION**

I **Vaibhav Budhiraja, 2K16/PTE/07** student of M.Tech hereby declare that the project Dissertation titled “**Chitosan Metal Oxides Based Nanocomposites for Biosensing Application**” which is submitted by me to the Department of Applied Chemistry, Delhi Technological University, Delhi in the partial fulfilment of the requirement for the award of the degree of Master of Technology, is original and not copied from any source without proper citation. This work has not previously formed the basis for the award of any Degree, Diploma Associateship, Fellowship or other similar title or recognition.

**Place:**

**Vaibhav Budhiraja**

**Date:**

**2K16/PTE/07**

Department of Applied Chemistry  
DELHI TECHNOLOGICAL UNIVERSITY  
(Formerly Delhi College of Engineering  
Bawana Road, Delhi-110042

**CERTIFICATE**

I hereby certify that the Project Dissertation titled “**Chitosan Metal Oxides Based Nanocomposites for Biosensing Application**” which is submitted by **Vaibhav Budhiraja, 2K16/PTE/07**, Department of Applied Chemistry, Delhi Technological University, Delhi in partial fulfillment of the requirement for the award of the Master of Technology, is a record of the project work carried out by the student under my supervision. To the best of my knowledge this work has not been submitted in part or full for any Degree or Diploma to this University or elsewhere.

**Place:**

**Dr. Chandra Mouli Pandey**

**Date:**

**(SUPERVISOR)**

**Place:**

**Dr. Saurabh Mehta**

**Date:**

**(SUPERVISOR)**

## ABSTRACT

Detection of xanthine is an important biomarker as a sign of spoilage. In this work efforts have been made to fabricate a xanthine biosensor based on chitosan (CH) metal oxides (ZnO, TiO<sub>2</sub> and MnO<sub>2</sub>), nanocomposite. The nanocomposites CH-ZnO, CH-TiO<sub>2</sub>, CH-MnO<sub>2</sub> were deposited on indium tin oxide (ITO) coated glass substrate by electrophoretic deposition process and xanthine oxidase enzyme (XO<sub>x</sub>) was immobilized on them using glutaraldehyde as crosslinking agent. Out of these three electrodes, CH-TiO<sub>2</sub>/ITO electrode was chosen for further studies due to its superior electrochemical properties compared to CH-ZnO/ITO and CH-MnO<sub>2</sub>/ITO electrode. The electrochemical response of the XO<sub>x</sub>/CH-TiO<sub>2</sub>/ITO bioelectrode show high sensitivity 0.577 μA/mM or 1.15 μA/mMcm<sup>2</sup>, short response time 60 s, linear response in the xanthine concentration range from 10μM – 250μM with a detection limit of 10 μM. Further, the fabricated biosensor has been utilized to confirm xanthine in a fresh Catla (*Labeo catla*) fish meat sample and proved to be a simple, reliable and economical method to evaluate freshness of fish.

## ACKNOWLEDGEMENT

The success and final outcome of this project required a lot of guidance and assistance from many people and I am extremely fortunate to have got this all along the completion of this project work.

I wish to express my gratitude towards my project supervisor and mentor, **Dr. Chandra Mouli Pandey and Dr. Saurabh Mehta, Department of Applied Chemistry and Polymer Technology, Delhi Technological University**, who provided me a golden opportunity to work under their able guidance. His scholastic guidance and sagacious suggestions helped me to complete the project on time.

I wish to thank **Dr. Archana Rani, Professor, Head of the Department of Applied Chemistry and Polymer Technology, Delhi Technological University** for his constant motivation and for providing able guidance.

I am thankful to and fortunate enough to get constant encouragement, support and guidance from all teaching as well as non-teaching staffs of Department of Applied Chemistry and Polymer Technology, which helped me in successfully completing my project work.

Finally, yet importantly, I would like to express my heartfelt thanks to my beloved family and friends who have endured my long working hours and whose motivation kept me going.

**VAIBHAV BUDHIRAJA**

## **List of Contents**

Candidate's Declaration	i
Certificate	ii
Acknowledgement	iii
Abstract	iv
Contents	v
List of Tables	vii
List of Figures	viii
List of Abbreviations	ix

### **CHAPTER 1. LITERATURE REVIEW**

<b>1.</b>	Introduction	1
<b>1.1</b>	Importance of Sensor	2
<b>1.1.1</b>	Biosensor	3
<b>1.2</b>	Introduction of Chitosan	4
<b>1.2.1</b>	Sources and chemical composition	5
<b>1.2.2</b>	Chemical Properties of Chitosan	7
<b>1.2.3</b>	Biological Properties of Chitosan	7
<b>1.3</b>	Nanostructured Materials	7
<b>1.3.1</b>	ZnO	8
<b>1.3.2</b>	TiO <sub>2</sub>	8
<b>1.3.3</b>	MnO <sub>2</sub>	9
<b>1.4</b>	Nanotechnology Enabled Sensors	9
<b>1.5</b>	Electrophoretic deposition	11
<b>1.5.1</b>	Properties of Electrophoretic deposition	12
<b>1.5.2</b>	Chitosan film	12

## **CHAPTER 2. EXPERIMENTAL WORK**

<b>2.1</b>	Materials Required	13
<b>2.2</b>	Synthesis of ZnO nanoparticles	13
<b>2.3</b>	Synthesis of TiO <sub>2</sub> nanoparticles	13
<b>2.4</b>	Synthesis of MnO <sub>2</sub> nanoparticles	14
<b>2.5</b>	Synthesis of Chitosan-Metal Oxides Nanocomposites	14
<b>2.6</b>	Electrophoretic deposition of CH-MOs blend film	14
<b>2.7</b>	Preparation of fish sample for real sample analyses	15

## **CHAPTER 3. RESULTS AND DISCUSSION**

<b>3.1</b>	FTIR of ZnO	16
<b>3.2</b>	FTIR of TiO <sub>2</sub>	17
<b>3.3</b>	FTIR of MnO <sub>2</sub>	18
<b>3.4</b>	FTIR of Chitosan	19
<b>3.5</b>	FTIR of CH-ZnO	20
<b>3.6</b>	FTIR of CH-TiO <sub>2</sub>	21
<b>3.7</b>	FTIR of CH-MnO <sub>2</sub>	22
<b>3.8</b>	SEM of Chitosan	23
<b>3.9</b>	SEM of CH-ZnO	23
<b>3.10</b>	SEM of CH-TiO <sub>2</sub>	24
<b>3.11</b>	SEM of CH-MnO <sub>2</sub>	24
<b>3.12</b>	CV for Chitosan	25
<b>3.13</b>	CV of electrodes (ITO, CH-TiO <sub>2</sub> /ITO, and XO <sub>x</sub> /CH-TiO <sub>2</sub> /ITO)	26

<b>3.14</b>	<b>Kinetics Parameters</b>	27
	<b>CHAPTER 4. CONCLUSION</b>	33
	<b>CHAPTER 5. REFERENCES</b>	34



## **List of Tables**

<b>Table 1.1</b>	Physiochemical characteristics of chitosan and their methods of determination.	6
<b>Table 3.14</b>	Change in current with respect to change in Xanthine concentration in <i>catla</i> fish sample	32

## **List of Figures**

<b>Fig. 1.1</b>	Scheme showing the fabrication of chitosan metal oxide based biosensor for Xanthine detection	2
<b>Fig. 1.2</b>	Schematic of a feedback sensing control system	4
<b>Fig. 1.3</b>	Chitosan process flow chart	6
<b>Fig.1.4</b>	Scheme showing the electrophoretic deposition process	11
<b>Fig. 3.1</b>	FTIR spectra of ZnO	16
<b>Fig. 3.2</b>	FTIR spectra of TiO <sub>2</sub>	17
<b>Fig 3.3</b>	FTIR spectra of MnO <sub>2</sub>	18
<b>Fig.3.4</b>	FTIR spectra of chitosan	19
<b>Fig. 3.5</b>	FTIR spectra of CH-ZnO	20
<b>Fig. 3.6</b>	FTIR spectra of CH-TiO <sub>2</sub>	21
<b>Fig. 3.7</b>	FTIR spectra of CH-MnO <sub>2</sub>	22
<b>Fig 3.8</b>	SEM of CH/ITO electrode	23
<b>Fig. 3.9</b>	SEM of CH-ZnO/ ITO electrode	23
<b>Fig. 3.10</b>	SEM image of CH-TiO <sub>2</sub> /ITO electrode	24
<b>Fig. 3.11</b>	SEM image of CH-MnO <sub>2</sub> /ITO electrode	24
<b>Fig. 3.12</b>	CV for chitosan on increasing scan rate from 10 to 250 (a–m), in phosphate buffer solution (50mM, pH 7) containing 0.9% NaCl	25
<b>Fig 3.13</b>	CV of electrodes (ITO, CH-TiO <sub>2</sub> /ITO, and XO <sub>x</sub> /CH-TiO <sub>2</sub> /ITO)	26

<b>Fig. 3.14</b>	Magnitude of current v/s potential difference as function of log of scan rate	28
<b>Fig. 3.15</b>	Magnitude of current v/s potential difference as function of square root of scan rate	29
<b>Fig. 3.16</b>	DPV of $XO_x/CH-TiO_2/ITO$ bioelectrode	30
<b>Fig. 3.17</b>	Linear plot of Current v/s log of concentration of Xanthine	31

## **List of Abbreviations**

CH	Chitosan
CV	Cyclic Voltammetry
DPV	Differential Pulse Voltammetry
EPD	Electrophoretic deposition
FTIR	Fourier-transform infrared spectroscopy
ITO	Indium Tin Oxide
MnO <sub>2</sub>	Manganese Oxide
MOs	Metal Oxides
PBS	Phosphate Buffer Solution
SEM	Scanning electron microscope
TiO <sub>2</sub>	Titanium Oxide
XO <sub>x</sub>	Xanthine Oxidase Enzyme
ZnO	Zinc Oxide

## 1. Introduction

In the last decade, there has been a great demand of biosensors for detection of xanthine because of their applications in the field of food and pharmaceutical industry [1-2]. Quantitative detection of xanthine helps us to estimate freshness of fish. Numerous methods such as, chemiluminescence, spectrophotometry, HPLC etc., have been utilized for xanthine detection. But these standard techniques are complex, time consuming and costly. In recent past, a lot of research has been done using electrochemical detection analysis, as it provide various advantages like high sensitivity, high specificity, less time and simple procedure [3]. Recently, the area of nanotechnology has provided new opportunities to discover various analytical applications of the nanostructured materials. Among the various nanomaterials, nanostructured metal oxides (NMOs) have been widely used in biosensor fabrication as they effectively mediate the electrons between the electrode and the biomolecule [4]. Further, NMOs provides high surface area and multiple active sites for the immobilization of biomolecules. Now a day's nanostructured  $\text{TiO}_2$  had been widely used in sensor fabrication as they provide high surface area, better electron transfer, non toxicity and biocompatibility. [5].

Xanthine is a produce due to the degradation of nucleotides in dead fish and its concentration increases with passage of time [7-8]. The detection of xanthine has is very important for the quality control of fish products in market. Very few literatures are available on detection of Xanthine in fish using a biosensor. [6].

In the present work a nanointerfaced biosensor based on CH/ $\text{TiO}_2$  nanocomposite has been fabricated that shows detection in the micromolar range and can be used for early detection of degraded Catla (*Labeo catla*) fish. Xanthine oxidase has been covalently immobilized onto the working electrode. The fabricated biosensor shows better performance in terms of sensitivity, linear range and time.

Xanthine is the precursor of uric acid. The basic electrochemical reactions involved in response measurement of xanthine biosensor are given below.  $\text{XO}_x$  immobilized onto CH- $\text{TiO}_2$ /ITO electrode yield flow of electrons by generating  $\text{H}_2\text{O}_2$  from xanthine. This flow of electrons is directly proportional to xanthine concentration.

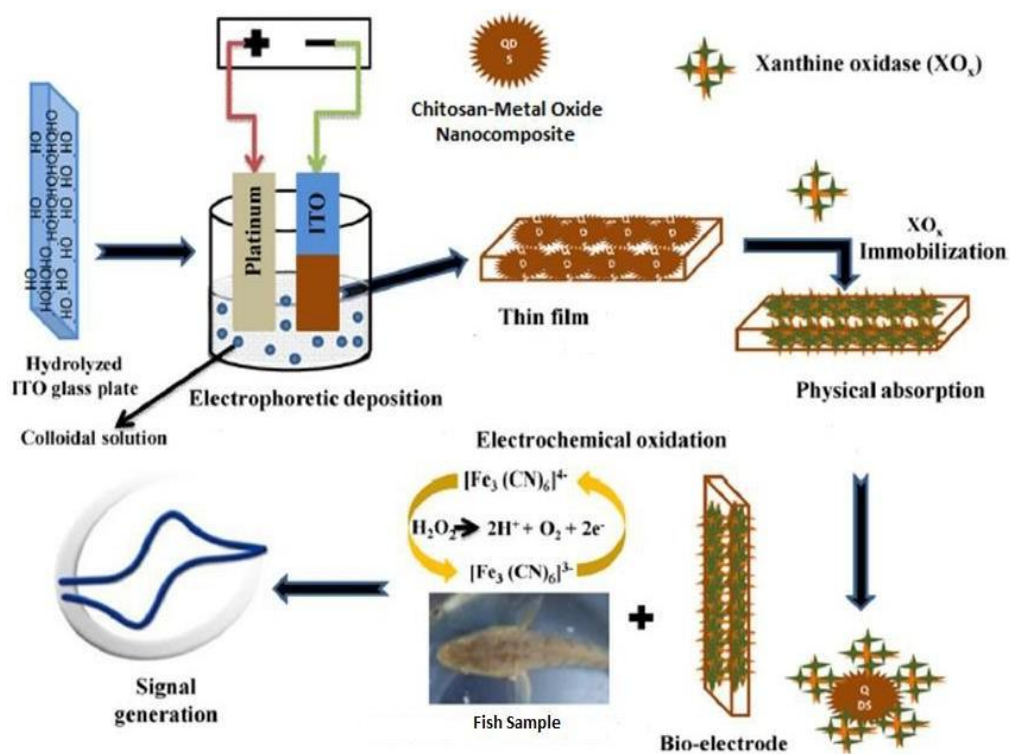
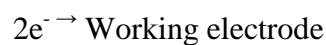
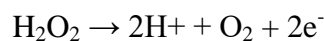
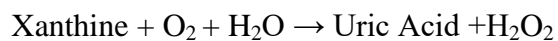


**Fig. 1.1 Scheme showing the fabrication of chitosan metal oxide based biosensor for Xanthine detection**

### 1.1 Importance of Sensor

The demand for sensor development to provide accurate, real-time information is increasing day by day. Most of the applications in areas like health care, veterinary research require specific real time monitoring, control to enhance efficiency, keep up health and safety. It provides information that is not available from analytical instruments such as the how the target species concentration varies in real time.

Figure 1.2 shows scheme of feedback sensing control system where, the chemical signal is transformed into electrical signal with the help of sensor, while the electrical signal is transformed into chemical signal by actuator. Sensors are exposed to the analyte for direct interaction with the target species. Thus, sensor technology has helped in achieving satisfactory stability, selectivity, reproducibility, and sensitivity at reasonable cost.

### **1.1.1 Biosensor**

A biosensor must have the following beneficial features:

- The biomolecules should be specific and steady at normal storage conditions for a particular analysis.
- The biomolecular reaction should be independent of pH, temperature etc. to have minimal pre-treatment before analysis. Involvement of any coenzymes in the reaction should be co-immobilized with the enzyme.[7-8]
- Response should be precise, linear, specific and free from electrical noise, without dilution or change in concentration.
- The biosensor used for invasive monitoring, must have small and biocompatible probe without any toxicity. For fermenters application it needs to be serialized by autoclaving.
- The complete biosensor must be small, user friendly and economical.

Thus, the demand of new sensors with better properties is growing day by day. To achieve it focus is on numerous approaches like research on novel sensing materials, surface modification, catalysts and promoters, optimization of sensor performance, data processing methods, fabrication techniques and nanotechnology. Various transducing platforms such as electrochemical, mass spectroscopic etc are also being utilize for sensing mechanism. [9]

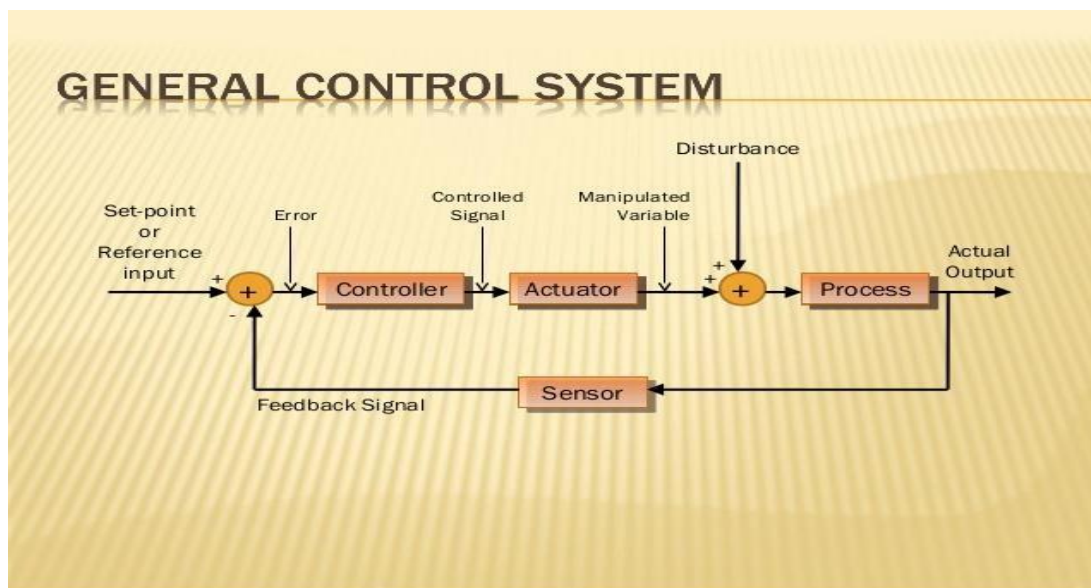


**Fig. 1.2 Schematic of a feedback sensing control system**

## 1.2 Introduction of Chitosan

Chitosan is the derivative of chitin obtained through enzymatic or chemical deacetylation. Chitin is a long chain polymer of  $\beta$ -(1-4) glucosamine with a number of N-acetyl groups. Until 1980 not much of research was done on chitin due to its complex structure, complex extraction and limited solubility in aqueous solutions.

Chitosan constitute of  $\beta$ -(1-4)-linked D-glucosamine and N-acetyl-D-glucosamine which is randomly dispersed in the polymer. In acidic environment, majorities of polysaccharides are either neutral or negatively charged, but chitosan is cationic in



nature. This cationic nature of chitosan helps in the formation of electrostatic complex with other negatively charged materials. The admirable properties of chitosan such as non-toxicity, biocompatibility, and biodegradability for various biomedical applications. These properties are affected by the degree of deacetylation, that depends on the molecular weight of chitosan and molar fraction of deacetylation. Due to this unique feature chitosan is widely used in tissue engineering, pharmaceuticals and biomedical applications [12].

### **1.2.1 Sources and Chemical Composition**

Chitin is a naturally occurring substance found in the shells of crustaceans, invertebrates, and fungi from which chitosan is derived by deacetylation process. Chitin is a linear polysaccharide comprised of *N*-acetyl- D-glucosamine chains  $\beta$  (1– 4)-2-acetamide-2-deoxy-D-glucose. It is like unramified cellulose and is insoluble in water. After deacetylation with NaOH, the resulting chitosan becomes soluble in acid, such as is present in the stomach. Once solubilized, the chitosan forms a gellike substance that binds lipids in the gastrointestinal tract, resulting in their fecal elimination. A new form of chitosan has been extracted and purified. This electrostatically charged chitosan is weakly absorbed systemically but is able to bind lipids and prevent their digestion. [13] The positively charged amino groups on the chitosan molecule bind to the negatively charged carboxylic groups of free fatty acids. This electromagnetic bond is stronger than those observed in other dietary fibers. Additionally, hydrophobic bonds are also formed between chitosan and neutral fats such as cholesterol and triglycerides. The modification of chitosan at atomic/molecular level enhances its stability and solubility, making it ideal as a biopolymer. Further free amino groups of chitosan can be modified in mild acidic conditions. Chitosan is usually converted into its derivatives or composites by reacting with other small molecules [15-16].

**Table 1.1 Physiochemical characteristics of chitosan and their methods of determination**

Physiochemical Characteristics	Method of Determination
Molecular Weight	viscometry; gel permeation chromatography; light scattering; highperformance liquid chromatography; matrix-assisted laser desorption/ionization-mass spectrometer
Degree of Deacetylation	infrared spectroscopy; ultra violet spectrophotometry; nuclear magnetic resonance spectroscopy ( $^1\text{H-NMR}$ and $^{13}\text{C-NMR}$ ); conductometric titration; potentiometric titration; differential scanning calorimetry
Crystallinity	X-ray diffraction

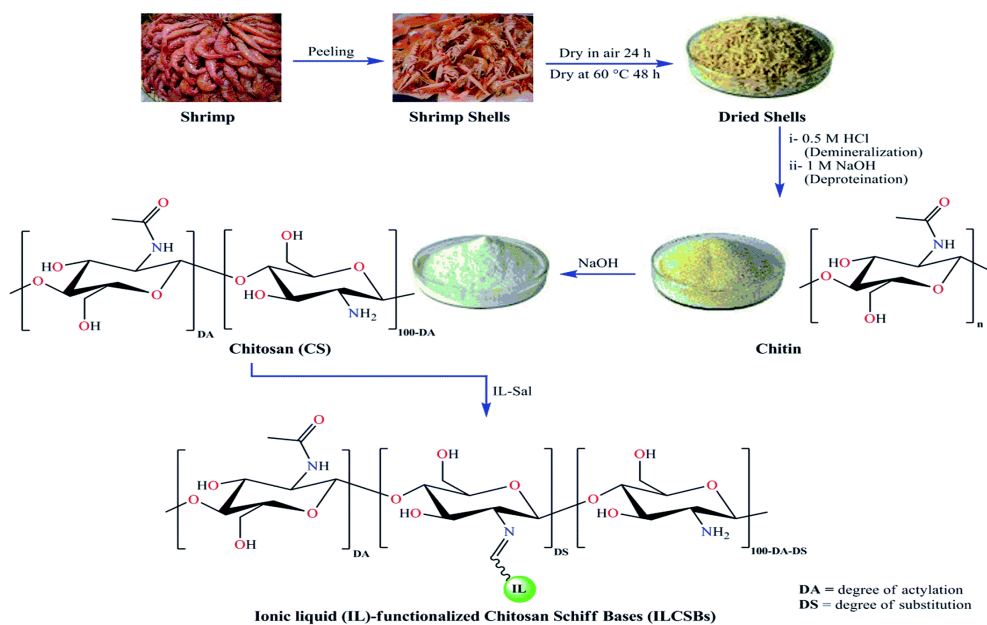


**Fig. 1.3 Chitosan process flow chart**

### **1.2.2 Chemical properties of chitosan**

The chemical properties of chitosan make it an appropriate material for biomedical application. Few properties are listed below;

- Linear polyamine
- Reactive amino groups (-NH<sub>2</sub>) and hydroxyl groups (-OH)
- Chelating compounds with transitional metal ions

### **1.2.3 Biological properties of chitosan**

Chitosan also have diverse biological properties that are listed below;

- Biocompatible
- Natural polymer
- Nontoxic
- Biodegradable
- Binds to microbial and mammalian cells
- Regenerative effect on gum tissue
- Help in bone formation by accelerating the formation of osteoblast.

## **1.3 Nanostructured Materials**

Recently research activities have been done for exploring structural characterization, synthesis and properties of nanostructured materials. Nanostructured materials display novel properties due to their small size [17]. It has been observed that electrical, optical, physical, magnetic and mechanical properties changes at the nanoscale regime. Nanosensors is one of the application of nanostructured materials that may include highly sensitive biosensors, gas sensors etc [18-21].

Nanostructured metal oxides in the form of nanoparticles, nanobelts and nanowires [22], greatly increase the response of sensors, because of high porosity, granularity and surface area to volume ratio of the sensing materials. It is well-known that sensitivity of

metal oxide is inversely proportional to the grain size [23]. Therefore nanostructured materials helps in fast response time and reaction compared to polycrystallite structures due to high surface to volume ratio.

### **1.3.1 ZnO**

ZnO is widely used semiconductor metal oxide and is extensively functional sensing material because of fast moving conducting electrons and excellent optical, thermal and chemical properties [24]. ZnO in nanostructured form i.e. nanowire and nanobelt is of great significance to develop sensitive sensors. ZnO have a distinct structural morphology of nanorods having hexagonal cross section and nanobelts having rectangular cross section. Its consistent structure makes it a suitable candidate for the fabrication of sensors [25]. Moreover, permeable structure is formed by thin film deposition of nanobelts and nanorods. Their large surface to volume ratios results in high sensitivity and response time [26].

### **1.3.2 TiO<sub>2</sub>**

TiO<sub>2</sub> nanoparticles have unique properties like high wide band gap, mechanical strength, biocompatibility, retention of biological activities and oxygen ion conductivity. Nanoporous TiO<sub>2</sub> electrodes has been engaged for electron transfer mechanisms of hydrogen peroxide in various bio active molecules, such as l-tyrosine, 3,4-dihydroxyphenylacetic acid etc. TiO<sub>2</sub> nanotube based sensors shows prominent result for sensing. The TiO<sub>2</sub> nanotube arrays are fabricated in an aq. electrolyte solution that contains hydrofluoric acid and acetic acid by anodizing titanium foil.[27]

### 1.3.3 MnO<sub>2</sub>

MnO<sub>2</sub> is favorable due to its low-cost and physicochemical properties. Manganese dioxide is an attractive inorganic material used in energy storage, catalysis and molecular adsorption. Besides, has also been widely used in biosensors. However, the application of MnO<sub>2</sub> is limited due to low electrical conductivity. [28]

The demand to combine inorganic materials with organic materials is very high for their extraordinary applications in electronics. Nanostructured metal oxides and chitosan increase the sensitivity. Such composites can easily be operated at room temperature and are highly selectivity towards various substrates. Moreover, the composite have long term stability and reproducibility. At nanometer scale the composite of organic and inorganic materials is considered as bi-phase materials. The properties of nanocomposite depend on their individual and shared properties [29].

### 1.4 Nanotechnology Enabled Sensors

Nanotechnology control phenomenon and properties of materials at the molecular and atomic level, which enables us to generate devices with better applications [30]. Nanotechnology offers an exclusive advantage to measure sensing at the molecular level by manipulating, fabricating and arranging materials. High percentage of active surface atoms of nanostructured materials maximize sensor output signal and helps in detection at molecular changes, compared to devices based on crystalline materials [31]. Thus, they help in increasing specificity of analyte by providing large number of binding sites for functionalization at their surface.

There is a huge challenge to improve the performance of sensor by exploring the advantages from nanotechnology like manufacturing nanostructures, controlling performance from in the nano scale, and evaluating reliable response. The development of nanostructured materials, must take into account the reality imposed by biology, chemistry, engineering, materials science and physics.

The basic aspects of nanostructured materials and sensors based on nanotechnology were discussed regarding sensors and different sensing platforms. The following work will show the sensing mechanisms of chitosan and metal oxides based sensors based on the nano structure of these materials. Various transitional metal oxides are reported in literature that are used as sensing materials, however present work focuses on nanostructured metal oxides (ZnO, TiO<sub>2</sub> and MnO<sub>2</sub>). [32-33] Metal Oxides Chitosan based sensors function at room temperature. Thus, there is a growing interest to combine chitosan with metal oxides for better sensing applications.

Nanostructured materials have dimension between 1 and 100 nm, have established greater than ever attention for sensing applications. Depending on dimensions nanostructured material are classified into different categories such as zero dimensional material such as quantum dots, one-dimensional materials like nanowires, nanobelts etc. and two dimensional is films. Out of these, one dimensional nanostructures such as belts, tubes, rods, fibres and wires is the key focus of concentrated research for application of nanodevices [34-37].

Nanostructured materials made with the desired properties like size, crystal structure, morphology, orientation and chemical composition are promising and find huge applications. Therefore, synthesis of nanomaterials is one of the most important aspects in nanotechnology. Various techniques are being utilized to create one dimensional nanostructure. For example, the structure of nanofibers, nanowires and nanorods having a wide range of diameters and lengths. The length of nanorodes is in micrometers while the length of the nanofibers and nanowires having a range in few hundred of micrometers. Nanotubes have wire-like structure with empty cores. Nanobelts have length and widths ranging from tens to hundred of nanometers with an identical rectangular cross-section [38-39]. Many techniques have been proposed to design material at the nanoscale to fabricate highly sensitive, selective and efficient biosensor. In this context NMOs is gaining attention as immobilizing platform in biosensors.

Biosensors have emerged as a very exciting technique for qualitative and quantitative determination of various analytes for environmental, clinical, agricultural, food, or military applications [41-42]. For the fabrication of high-performance biosensors for clinical diagnostic applications, nanotechnology represents their improved or remarkable features that allow various industrial applications [43-44].

### 1.5 Electrophoretic deposition

In electrophoretic deposition process particles get suspended in a liquid medium and deposit on an electrode by migrating in an electric field. The principle is electric double layer growth of charge at the surface of particles. It affects the ions distributed on the surface, in the neighboring interfacial region which ultimately increases the concentration of counter ions.

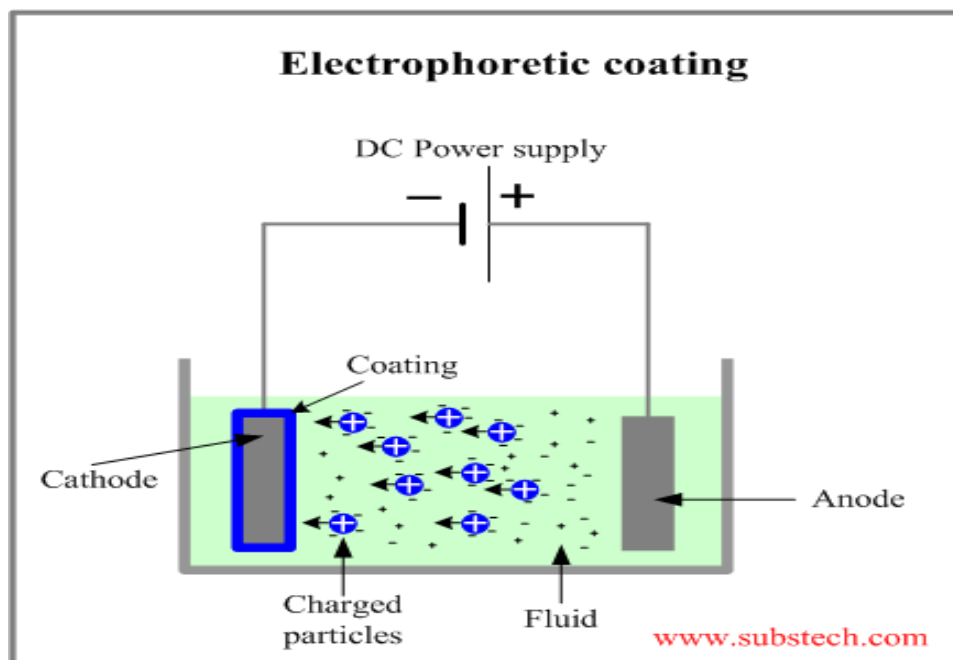


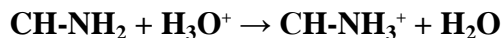
**Fig1.4** Scheme showing the electrophoretic deposition process

### 1.5.1 Properties of Electrophoretic deposition

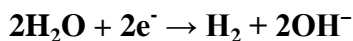
- The process gives a uniform and smooth coating of variable thickness exclusive of porosity.
- Coating of complex fabricated objects like composites, on both the surfaces.
- High speed of coating with relatively high purity than other conventional methods.
- Applicability to variety of materials such as polymers, ceramics and metals.
- Easy to access and control the coating composition.
- Automatic process that does not require high skills like other conventional coating processes.
- Coating materials are utilized very efficiently that result in lesser costs comparative to other processes.

### 1.5.2 Chitosan film

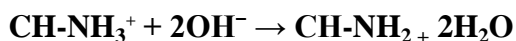
The significance in CH in the fabrication of film by EPD originated due to the cationic nature of this biopolymer and splendid film forming properties. Protonation in mild acidic solutions leads to water soluble and positively charged CH.



Precipitation of CH occurs due to increase in pH. At cathode surface pH increases due to reduction of water;



CH is deposited by the electrophoretic movement of positive charged CH and its neutralization in high pH. Insoluble CH films are formed by this process. [46].





## 2.0 EXPERIMENTAL WORK

### 2.1 Materials Required

Xanthine Oxidase, Chitosan (MW:  $2.4 \times 10^6$  Da), Zinc acetate dihydrate  $\text{Zn}(\text{CH}_3\text{COO})_2 \cdot 2\text{H}_2\text{O}$ , Tetraisopropylorthotitanate  $\text{Ti}(\text{OC}_3\text{H}_7)_4$  and Manganese acetate tetra-hydrate  $(\text{CH}_3\text{COO})_2\text{Mn} \cdot 4\text{H}_2\text{O}$  has been obtained from Sigma Aldrich. Sodium laureth sulfate and Ammonium Hydroxide were procured from SRL and Qualikems respectively. All other reagents like Hydrochloric acid, acetic acid, nitric acid etc. are of analytical grade. Methanol and ethanol were used as solvents. Distilled water is used to prepare all aqueous solutions.  $\text{Na}_2\text{HPO}_4$  and  $\text{NaH}_2\text{PO}_4$  are used to prepare Phosphate buffer solution (PBS).

### 2.2 Synthesis of ZnO nanoparticles

Zinc acetate dihydrate  $\text{Zn}(\text{CH}_3\text{COO})_2 \cdot 2\text{H}_2\text{O}$ , 1g is dissolved in 20ml ethanol at room temperature. Then 1M solution of NaOH is added drop wise to maintain pH 10 with constant stirring for 1 hour. White precipitate of  $\text{Zn}(\text{OH})_2$  obtained is washed with water to attain pH 7.0. Finally dil.  $\text{HNO}_3$  is added to get ZnO nanoparticles precipitates.

### 2.3 Synthesis of $\text{TiO}_2$ nanoparticles

10ml solution of Tetraisopropylorthotitanate  $\text{Ti}(\text{OC}_3\text{H}_7)_4$ , is dissolved in methanol and ethanol mixture having molar ratio (1: 1: 10) and refluxed for 6 hour at  $60^\circ\text{C}$ . Water is added drop wise to the solution and precipitate is filtered. The absorbed impurities are removed by washing with water and HCl and heated for 12 hour at  $130^\circ\text{C}$ .

## 2.4 Synthesis of MnO<sub>2</sub> nanoparticles

A transparent solution is obtained by dissolving 1.0 g sodium laureth sulfate in 80 ml ethanol at 25°C. 5ml conc. HNO<sub>3</sub> is added into the solution followed by 0.08 mol manganese acetate tetra-hydrate (CH<sub>3</sub>COO)<sub>2</sub>Mn.4H<sub>2</sub>O. The mixture is stirred until the manganese acetate gets dissolved completely and color becomes pale pink. Lastly, the solution is put for drying at 80°C for 48 h. The solution turns to black foam-like solid is washed with water and put in oven at 80°C for 24 h.

## 2.5 Synthesis of CH-MOs nanocomposites

50 mg of CH is dissolved in 100 mL of acetate buffer to get CH solution. To this solution 5 mg of metal oxides nanoparticles are dispersed via magnetic stirring at room temperature for 1h followed by sonication for around 4 h.

## 2.6 Electrophoretic deposition of CH-MOs blend film

ITO coated glass substrate are hydrolyzed before performing EDP. It is being immersed in H<sub>2</sub>O<sub>2</sub>/NH<sub>4</sub>OH/H<sub>2</sub>O solutions in ratio (1:1:5, v/v) at 80°C for 30 min. The electrophoretic deposition is done with 3ml of metal oxides/chitosan solution diluted with 9ml of ethanol. A thin film is cathodically deposited onto ITO electrode at 25V for 60 sec, using platinum as the counter electrode and Ag/AgCl as reference electrode. Three electrodes are made XO<sub>x</sub>/CH-ZnO/ITO, XO<sub>x</sub>/CH-TiO<sub>2</sub>/ITO and XO<sub>x</sub>/CH-MnO<sub>2</sub>/ITO, which are further studied for biosensing applications.

## **2.7 Preparation of fish sample for real sample analyses**

Xanthine detection in fresh Catla fish sample has been studied. The Catla fish is chopped into small pieces and homogenized in 5 ml 0.5 M HClO<sub>4</sub> to obtain a fine paste. The sample is firstly stirred for 15 min and centrifuged at 6000 rpm for 10 min. Fish meat extract is obtained by filtering through whatman filter paper and NaOH is added to it drop wise until pH reaches to 7.4. It is further stirred and diluted 10 times to the initial volume. The concentration of xanthine is determined from one part by DPV and the magnitude of current response is recorded upto 9 days.

### 3.0 RESULT AND DISCUSSION

#### 3.1 FTIR of ZnO

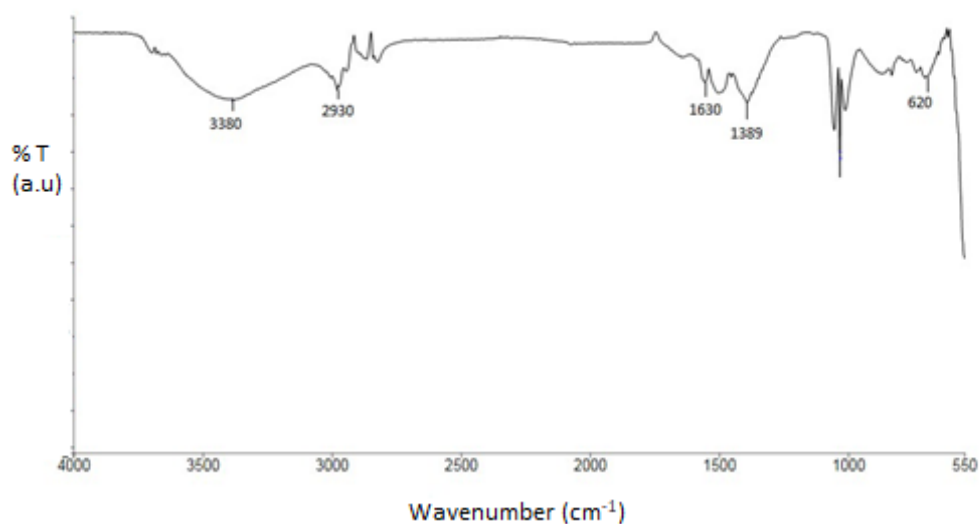


**Fig. 3.1 FTIR spectra of ZnO**

FTIR spectra of the ZnO sample show absorption peaks from 550 to 4000  $\text{cm}^{-1}$ . Peak at 2930  $\text{cm}^{-1}$  is assigned to C-H stretching vibration of alkane groups. A wide band at 3380  $\text{cm}^{-1}$  is attributed to the O-H bond of hydroxyl group. Symmetrical and asymmetrical stretching of the zinc carboxylate can be confirmed from peaks at 1384  $\text{cm}^{-1}$  and 1630  $\text{cm}^{-1}$ , respectively. Peak at 620  $\text{cm}^{-1}$  occurs due to oxygen deficiency/vacancy defect in ZnO.

### 3.2 FTIR of TiO<sub>2</sub>

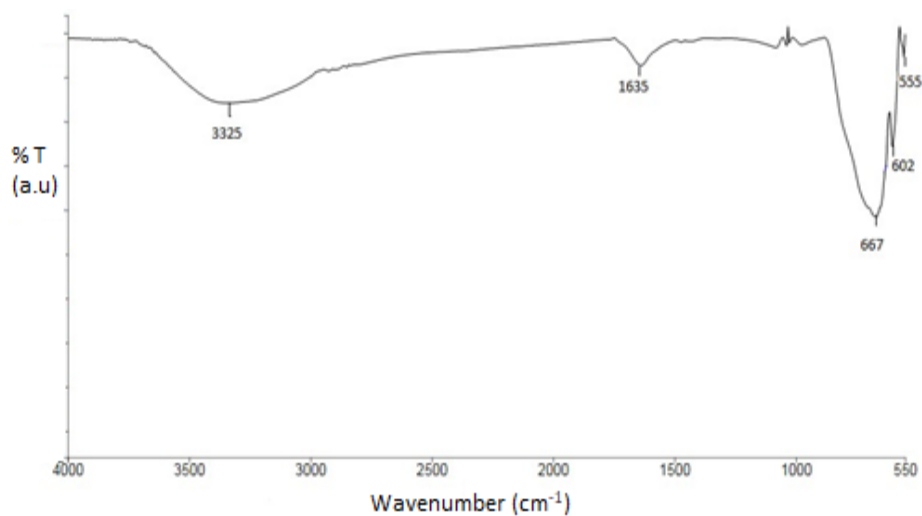


**Fig. 3.2 FTIR spectra of TiO<sub>2</sub>**

FTIR spectra of the TiO<sub>2</sub> sample show absorption peaks from 550 to 4000 cm<sup>-1</sup>. The wide band at 550-650 cm<sup>-1</sup> is attributed to the Ti-O bonds in TiO<sub>2</sub> lattice. The broad peaks appearing at 3324 cm<sup>-1</sup> and 1635 cm<sup>-1</sup> are due to interactions between hydroxyl groups with TiO<sub>2</sub>.

### 3.3 FTIR of MnO<sub>2</sub>

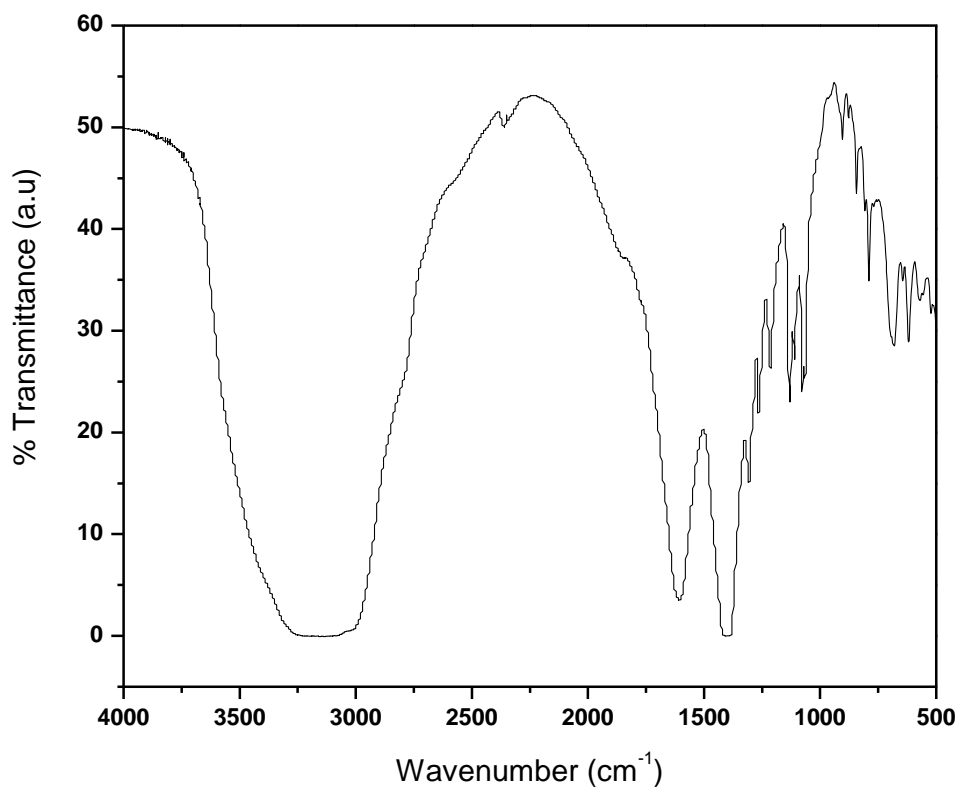


**Fig 3.3 FTIR spectra of MnO<sub>2</sub>**

FTIR spectra of the MnO<sub>2</sub> sample show absorption peaks from 500 to 4000 cm<sup>-1</sup>. The band at 549 cm<sup>-1</sup> is attributed to the Mn-O bonds in MnO<sub>2</sub> lattice. The wide band at 3140 cm<sup>-1</sup> is due to hydroxyl group of water molecules. In addition, the bands at 1601 and 1391 cm<sup>-1</sup> also confirms that water molecules are absorbed and imply the presence of large numbers of remaining hydroxyl groups with MnO<sub>2</sub>.

### 3.4 FTIR of Chitosan

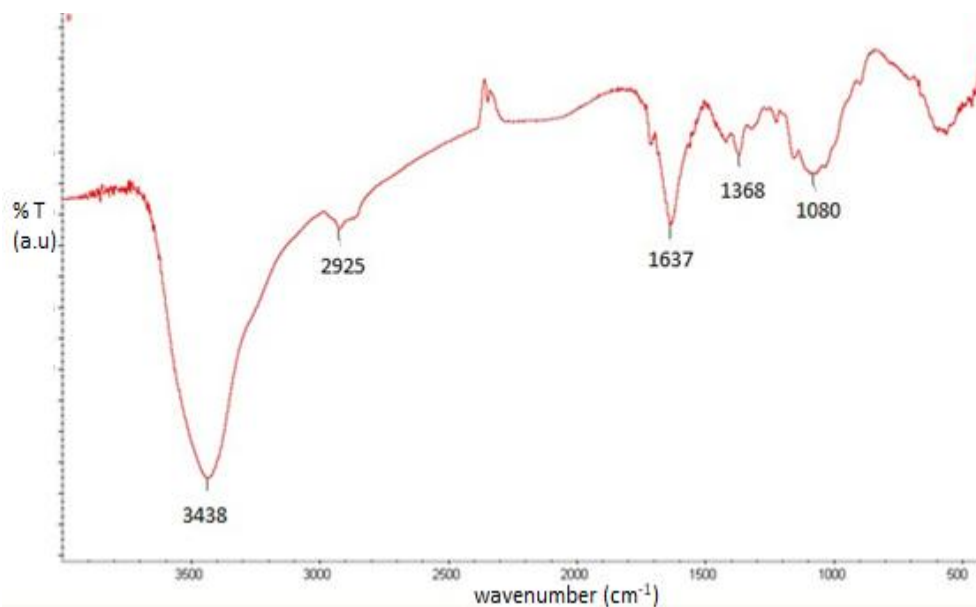


**Fig.3.4 FTIR spectra of chitosan**

FTIR spectra of the chitosan sample show absorption peaks from 500 to 4000  $\text{cm}^{-1}$ . Chitosan have absorption peak at 3438  $\text{cm}^{-1}$  is due to overlapping of the OH and  $\text{NH}_2$  stretches. The peak appearing at 2925  $\text{cm}^{-1}$  is due to C-H bond .The absorption peak at 1637  $\text{cm}^{-1}$  is attributed to carbonyl group and 1368  $\text{cm}^{-1}$  can be assigned to  $\text{CH}_2\text{OH}$ . Peak at 1080  $\text{cm}^{-1}$  corresponds to -C-O group.

### 3.5 FTIR of CH-ZnO

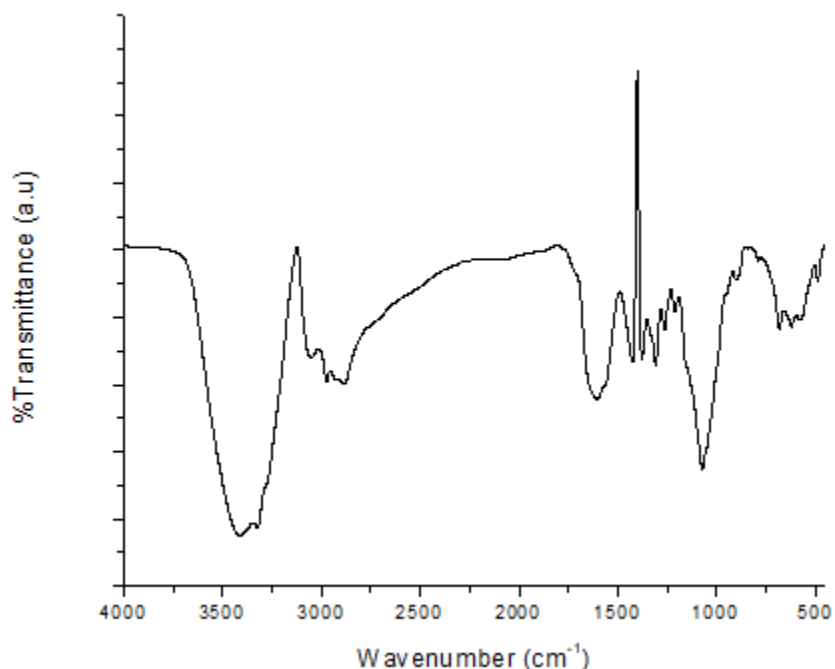


**Fig. 3.5 FTIR spectra of CH-ZnO**

FTIR spectra of the chitosan sample show absorption peaks from 500 to 4000  $\text{cm}^{-1}$ . Peak at 1377  $\text{cm}^{-1}$  has been assigned to the COO bond in carboxylic acid, 1425  $\text{cm}^{-1}$  showed the C-N of amine group. Peak at 1590  $\text{cm}^{-1}$  has been attributed to the -NH deformation, while 1071  $\text{cm}^{-1}$  is assigned to the C-O-C bond. Characteristic bands of both CH and ZnO are displayed. The band at 680  $\text{cm}^{-1}$  is of Zn-O in the matrix. On comparing with pure CH, strong interaction between the CH and ZnO nanoparticles is observed. As the bands related to amino, amide and hydroxyl groups in composite are shifted towards the lower wavenumber.



### 3.6 FTIR of CH-TiO<sub>2</sub>

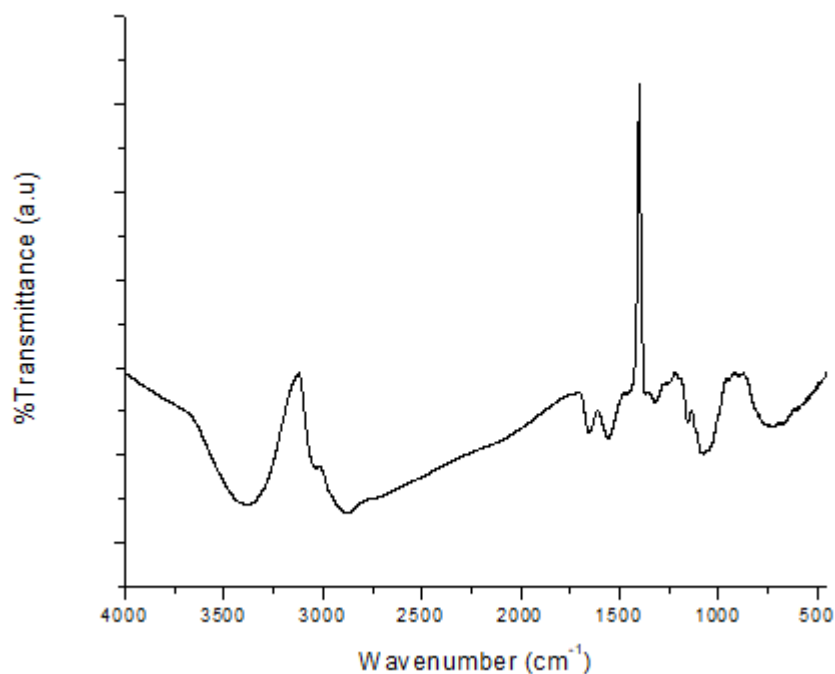


**Fig. 3.6 FTIR spectra of CH-TiO<sub>2</sub>**

FTIR spectra of the chitosan sample show absorption peaks from 500 to 4000  $\text{cm}^{-1}$ . For CH-TiO<sub>2</sub> composite, the peak at 1073  $\text{cm}^{-1}$  can be attributed to the C–O bond of CH. The peak at 725  $\text{cm}^{-1}$  is attributed to the COC group, while others at 1554, 1655 and 1319  $\text{cm}^{-1}$  are due to the N-H bending of the amines groups. The wide band at 3385  $\text{cm}^{-1}$  can be attributed to the O-H bond of chitosan. Peak at 2875  $\text{cm}^{-1}$  and 1389  $\text{cm}^{-1}$  is assigned to C-H bond and symmetric deformation mode of the CH<sub>3</sub> group. Finally a wide band below 950  $\text{cm}^{-1}$  is associated to the occurrence of Ti-O group in the composite.

### 3.7 FTIR of CH-MnO<sub>2</sub>

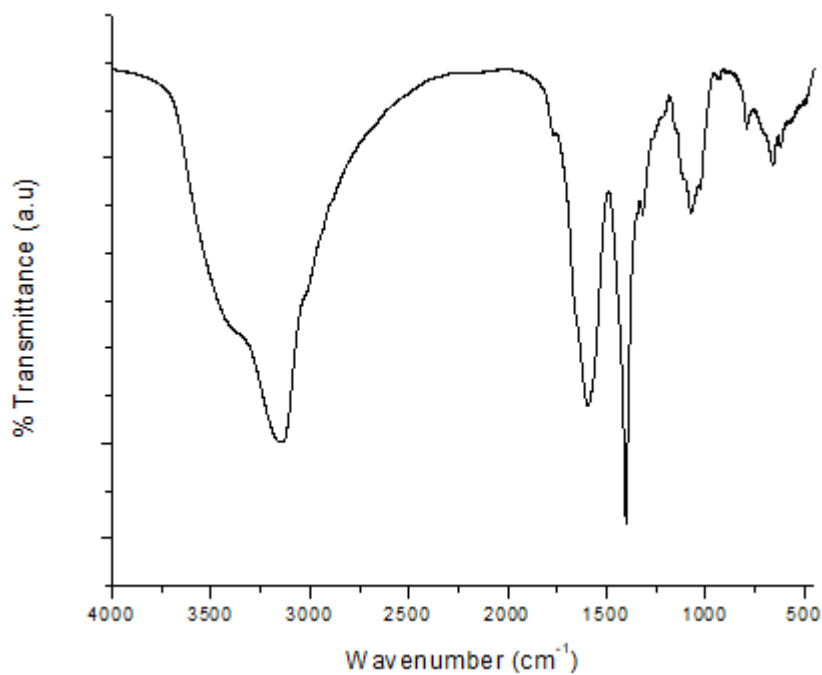


**Fig. 3.7 FTIR spectra of CH-MnO<sub>2</sub>**

FTIR spectra of the chitosan sample show absorption peaks from 500 to 4000  $\text{cm}^{-1}$ . The wider band at 3100-3400  $\text{cm}^{-1}$  corresponds to hydroxyl and amino groups of CH-MnO<sub>2</sub> film. The OH/NH group of chitosan binds with MnO<sub>2</sub> nanoparticles by hydrogen bonding. The peak at 660  $\text{cm}^{-1}$  is assigned to Mn-O bond and shows the deformation in the crystal structure of MnO<sub>2</sub>. It indicates the interaction of MnO<sub>2</sub> nanoparticles and CH matrix, forming a composite.

### 3.8 SEM of Chitosan

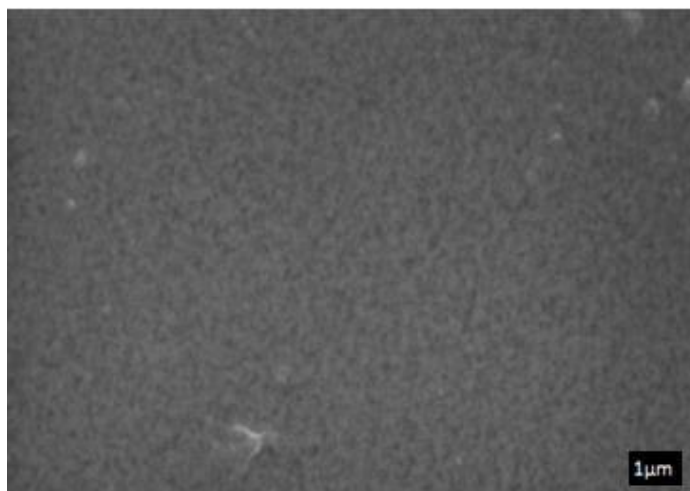


**Fig 3.8 SEM image of CH/ITO electrode**

Scanning electron microscope is used to study the surface morphology of CH which is electrophoretically deposited on ITO. A uniform CH film deposited with fine and crevice free surface is observed.

### 3.9 SEM of Chitosan-ZnO

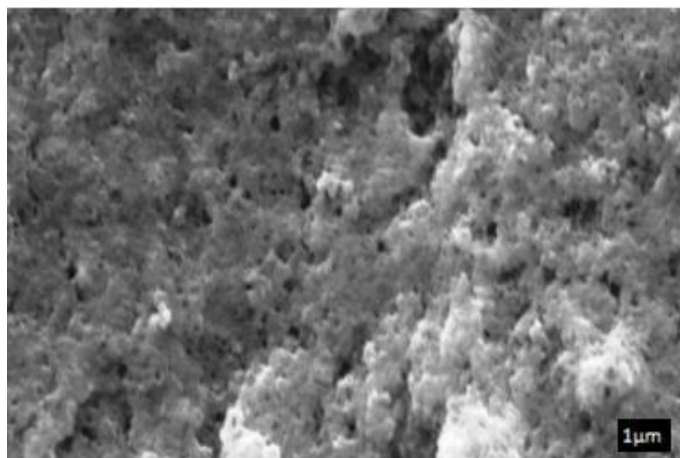


**Fig. 3.9 SEM image of CH-ZnO/ITO electrode**

CH-ZnO film shows agglomeration due to strong inter particle interactions.

### 3.10 SEM of Chitosan-TiO<sub>2</sub>

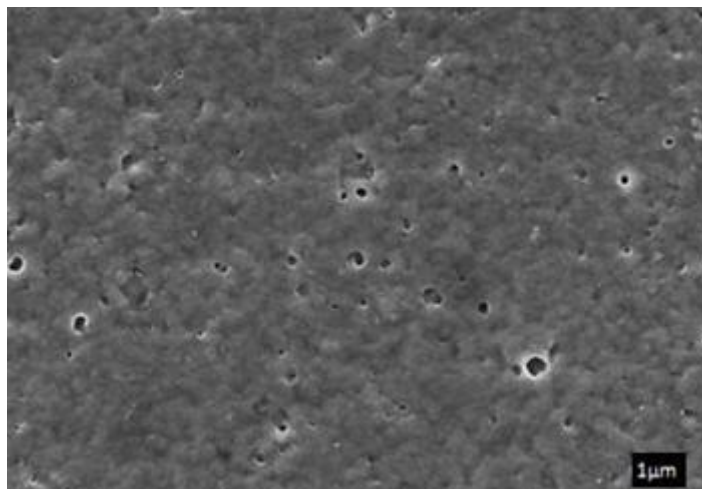


**Fig. 3.10 SEM image of CH-TiO<sub>2</sub>/ITO electrode**

CH-TiO<sub>2</sub> film show a uniform film with some minute pores of identical size spread over the surface. The surface of CH-TiO<sub>2</sub> matrix provides an excellent platform for immobilization of XO<sub>x</sub>.

### 3.11 SEM of Chitosan-MnO<sub>2</sub>

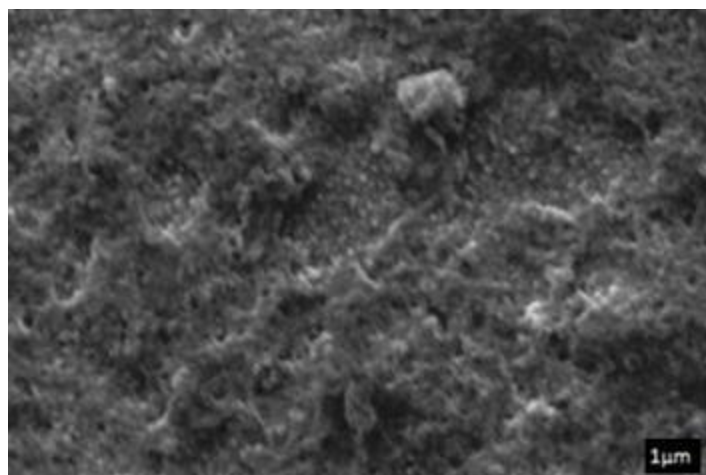


**Fig. 3.11 SEM image of CH-MnO<sub>2</sub>/ITO electrode**

A non uniform film of CH-MnO<sub>2</sub> showing the presence of MnO<sub>2</sub> cluster in CH. MnO<sub>2</sub> with some aggregation is uniformly impregnated in the CH network.

### 3.12 CV of Chitosan

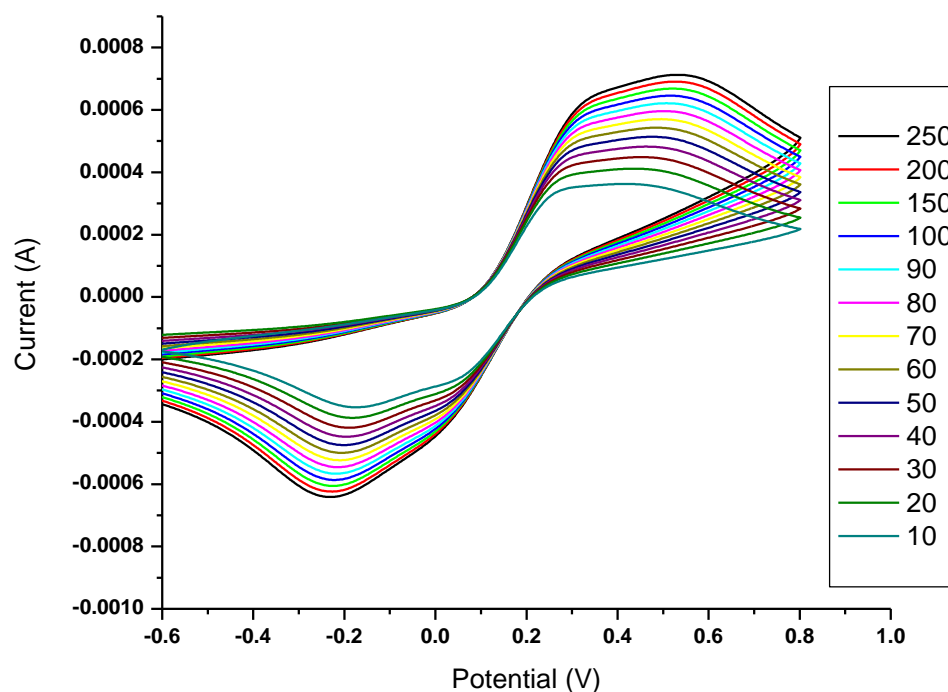


**Fig. 3.12 CV for chitosan on increasing scan rate from 10 to 250 (a–m), in phosphate buffer solution (50mM, pH 7) containing 0.9% NaCl**

The deposited Chitosan on ITO glass sheet is used for CV measurements. Measurements is carried out in a three-compartment cell containing 5mM Potassium ferri- and ferrocyanide buffer solution, working electrode, counter electrode and a reference electrode in the potential range from -0.6 to +1 V at a scan rate of 10, 20, 30, 40, 50, 60, 70, 80, 90, 100, 150, 200, 250  $\text{mV s}^{-1}$ . The cyclic voltammogram of pure Chitosan shows an oxidation peaks at 0.5V while the reduction peak is observed at -0.1V respectively. The redox processes gave roughly symmetric anodic peaks at different scan rates.

### 3.13 CV of electrodes (ITO, CH-TiO<sub>2</sub>/ITO, and XO<sub>x</sub>/CH-TiO<sub>2</sub>/ITO)

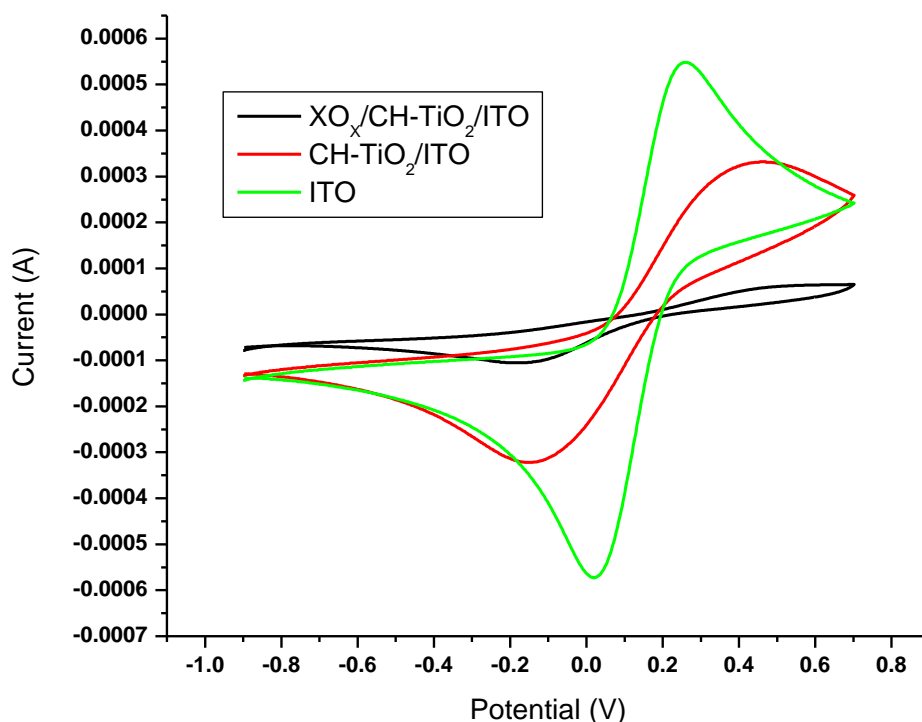


**Fig 3.13 CV of electrodes (ITO, CH-TiO<sub>2</sub>/ITO, and XO<sub>x</sub>/CH-TiO<sub>2</sub>/ITO)**

The results of CV studies shows that magnitude of the current ( $3.32 \times 10^{-4}$  mA) of CH-TiO<sub>2</sub>/ITO electrode is reduced as compared to bare ITO electrode ( $5.48 \times 10^{-4}$  mA) arising due to presence of non conducting chitosan. Due to poorer electron transfer decreased electron mobility at the surface of CH-TiO<sub>2</sub>/ITO electrode is observed that results in lower redox potential of CH-TiO<sub>2</sub>/ITO electrode. Immobilization of XO<sub>x</sub> onto CH-TiO<sub>2</sub>/ITO electrode, results in drastic decrease in the response of magnitude of current due to strong binding of XO<sub>x</sub> with the CH-TiO<sub>2</sub>/ITO electrode that hinders the movement of charge carrier. It seems that the insulating nature of XO<sub>x</sub> possibly disturb movement of electrons between the electrode XO<sub>x</sub>/CH-TiO<sub>2</sub>/ITO and the medium.

### 3.13 Kinetics Parameters

Since enzymes' activity is dependent on pH. The response of xanthine biosensor having pH between 5.0 and 9.0 is studied with the help of 0.05 mM xanthine in 50 mM PBS. The results indicate that there is increase in response from pH 5.0 to 7.4 and then a decrease in trend is found. The results suggested that pH 7.4 shows maximum response to the xanthine biosensor. Thus, further experiments are done at pH 7.4. The immobilization procedure of  $XO_x$  does not affect the pH 7.4.

The results of  $XO_x/CH-TiO_2/ITO$  electrode are shown. The reduction and oxidation reactions of the  $[Fe(CN)_6]^{3-/4-}$  redox pair corresponds to, negative and positive peaks respectively. For both oxidation and reduction peak currents  $I_p$  follow a linear relation with respect to the sq. root of scan rate (Fig. 3.15), that indicates controlled electrochemical reaction rates at the redox pair. With increase in scan rate the oxidation peak shifts towards a more positive value and reduction peak towards a more negative one. Both the peak potentials are linearly dependent on the log of the scan rate that increases with increase of the scan rate (Fig. 3.14), which is stated by Laviron's theory as follows:

$$E_{pa} = E^\circ + X \ln[(1-\alpha)Fv/RTk_s] \quad (1)$$

$$E_{pc} = E^\circ + Y \ln[(\alpha)Fv/RTk_s] \quad (2)$$

$$\ln k_s = \alpha \ln(1-\alpha) + (1-\alpha) \ln \alpha - \ln(RT/nFv) - \alpha(1-\alpha)nF\Delta E_p/RT \quad (3)$$

where  $k_s$  and  $\alpha$  are the charge transfer rate constant and the electron transfer coefficient respectively. The graph between  $\ln y$  v/s the cathodic peak potential ( $E_{pc}$ ) and anodic peak potential ( $E_{pa}$ ) yields two straight lines having slope  $Y=RT/\alpha nF$  and  $X= RT/(1-\alpha)nF$  respectively. With the help of plot and eqns (1) and (3), the values of  $k_s$  and  $\alpha$  is found to be  $21.77 \text{ s}^{-1}$  and 0.72 respectively.

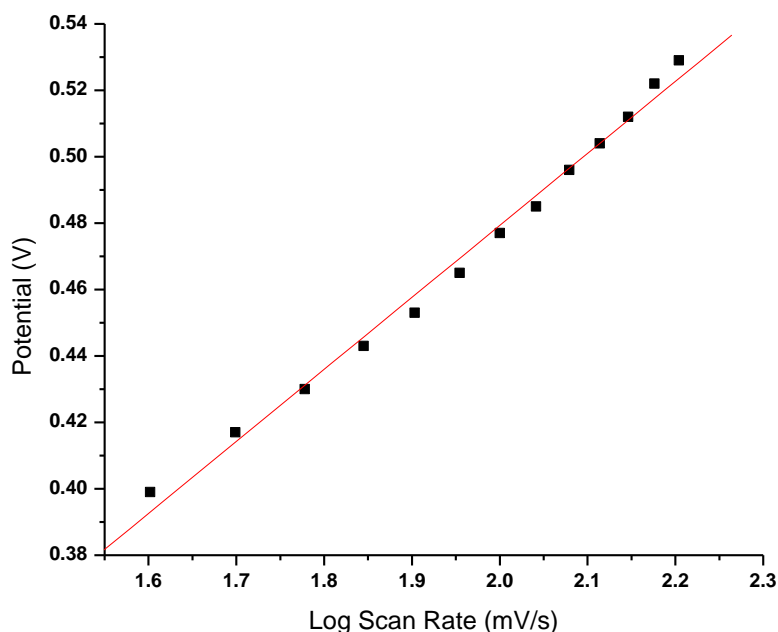


**Fig. 3.14 Magnitude of current v/s potential difference as function of log of scan rate**

Relationship between peak current ( $I_p$ ) and surface coverage is given according to Laviron's equation which is as follows;

$$I_p = n^2 F^2 \nu A \Gamma (4RT)^{-1} \quad (4)$$

where,  $n$  is the number of electrons transferred,  $A$  is the electrode area ( $0.50 \text{ cm}^2$ ),  $I_p$  is peak current,  $\nu$  is the scan rate ( $50 \text{ mV/s}$ ) and  $\Gamma$  is the average surface coverage of the electrode redox substance ( $\text{mol cm}^2$ ).  $\Gamma$  is found to be  $6 \times 10^{-12} \text{ mol cm}^{-2}$  which is calculated by taking the average of both the anodic and cathodic results.

According to the Randles-Sevcik equation, the linear slope of the anodic peak current on the sq, root of the potential sweep rate is given by,

$$I_p = (2.99 \times 10^5) \alpha^{1/2} n^{3/2} A C D^{1/2} \nu^{1/2} \quad (5)$$

the  $C$  is the molar concentration of  $[\text{Fe}(\text{CN})_6]^{3-/4-}$ ,  $\nu$  is the scan rate ( $50 \text{ mV s}^{-1}$ ),  $n$  is the number of transferred electrons for the redox reaction, diffusion coefficient ( $D$ ) is found



to be  $7.354 \times 10^{-15} \text{ cm}^2 \text{ s}^{-1}$ . By using eq. (6) and plot for  $I_p$  versus  $v^{1/2}$ , slope  $S$  is obtained and the effective surface area of the electrode ( $A$ ) is found to be  $0.501 \text{ mm}^2$ .

$$A = S / (2.99 \times 10^5) n^{3/2} a^{1/2} C D^{1/2} \quad (6)$$

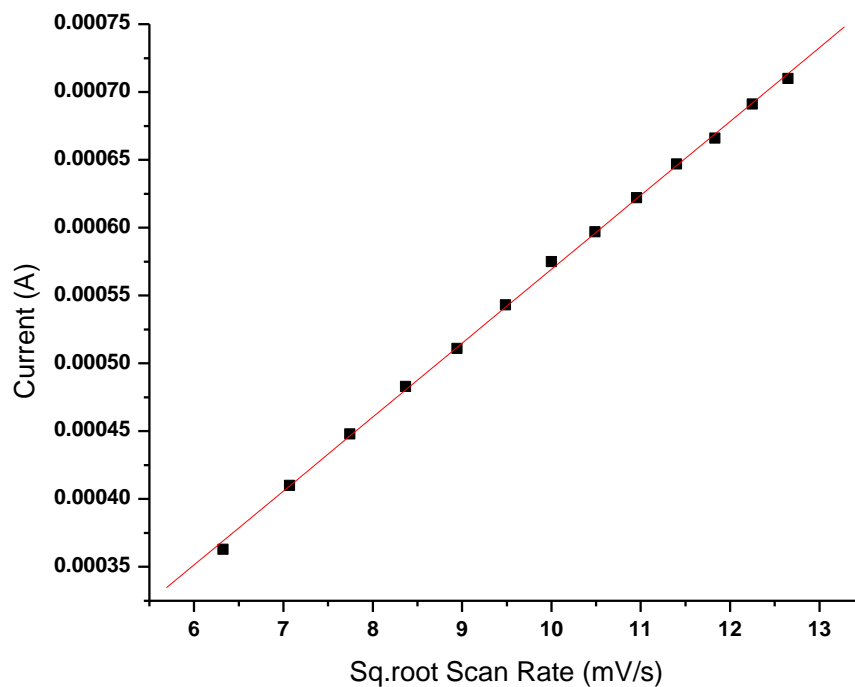


**Fig. 3.15** Magnitude of current  $v/s$  potential difference as function of square root of scan rate

**Table 3.13** Kinetic parameters calculated for the fabricated bioelectrodes

Sl. no	Name of the electrode	Electron transfer coefficient, $\alpha$	Charge transfer rate constant, $k_s/s^{-1}$	Effective surface area, $A_{eff}/\text{cm}^2$	Average surface coverage, $\Gamma/\text{mol cm}^{-2}$	Diffusion coefficient, $D/\text{cm}^2 \text{ s}^{-1}$
1.	XO <sub>x</sub> /CH-TiO <sub>2</sub> /ITO	0.72	21.77	0.501	$6.00 \times 10^{-12}$	$7.354 \times 10^{-15}$

The electrochemical response of the fabricated  $XO_x/CH-TiO_2/ITO$  electrode is examined using Differential pulse voltammetry (DPV) to detect Xanthine having concentration ranging from (10-250)  $\mu M$  Fig. 3.16. The incubation time of 5 min. is found enough for interaction of xanthine with the  $XO_x/CH-TiO_2/ITO$  electrode. The results suggested that the current decreases with increase in the concentration of Xanthine up to 250  $\mu M$  and remains constant thereafter. It proves that all the immobilized  $XO_x$  on electrode surface interacted with xanthine up to the concentration of 250  $\mu M$ .

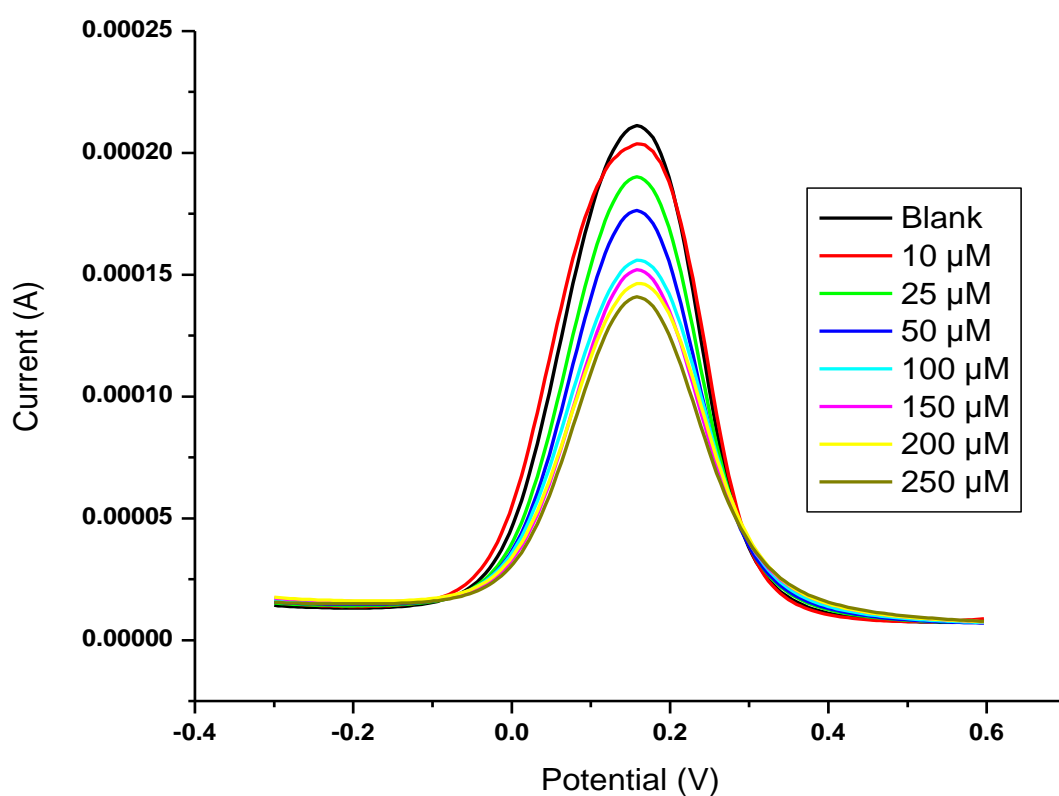


**Fig. 3.16 DPV of  $XO_x/CH-TiO_2/ITO$  bioelectrode**

The reduction of  $XO_x$  giving rise to reduction current peak is found to be proportional to the conc. of the xanthine on the logarithmic scale Fig.3.17. Sensitivity of electrode is found to be  $0.577 \mu\text{A}/\text{mM}$  or  $1.15 \mu\text{A}/\text{mMcm}^2$ .

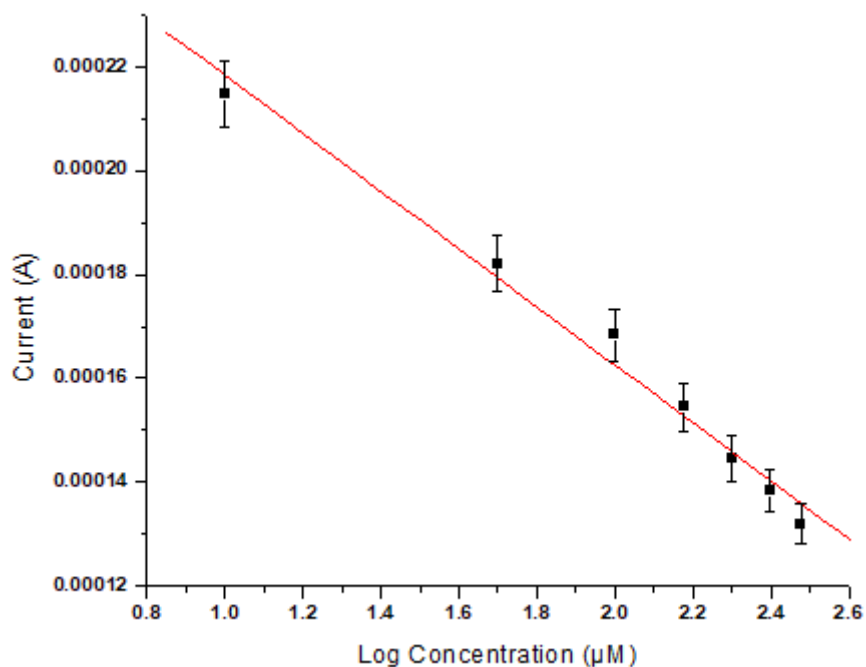


**Fig 3.17 Linear plot of Current v/s log of concentration of Xanthine**

The following table shows the variation in current observed in fresh catla fish meat sample. The homogenized solution is prepared by cutting catla fish into small pieces and interaction of electrode is recorded over a period of nine days. It is being found that on day 1 the current is high ( $1.632 \times 10^{-4}$  A), that decreases subsequently after keeping it in refrigerator at a temperature of  $4^\circ\text{C}$ . The results indicate that the current reduces to ( $1.392 \times 10^{-4}$  A) on 9<sup>th</sup> day that reveals the interaction of electrode with increase in the concentration of xanthine.

**Table 3.14 Change in current with respect to change in Xanthine concentration in catla fish sample**

<b>S.No</b>	<b>Time Period (Day)</b>	<b>Current (A)</b>
1	Day 1	$1.632 \times 10^{-4}$
2	Day 2	$1.579 \times 10^{-4}$
3	Day 3	$1.537 \times 10^{-4}$
4	Day 4	$1.513 \times 10^{-4}$
5	Day 7	$1.470 \times 10^{-4}$
6	Day 8	$1.431 \times 10^{-4}$
7	Day 9	$1.392 \times 10^{-4}$

## 4. CONCLUSION

Titanium oxide nanoparticles have been impregnated into CH matrix and immobilization of  $XO_x$  has been done in CH-TiO<sub>2</sub>/ITO electrode. Chitosan do not affect the physical properties of TiO<sub>2</sub> and provide high surface area for immobilization of  $XO_x$ . The immobilized  $XO_x$  shows outstanding properties towards biosensing interface composite of CH-TiO<sub>2</sub> and improves electron transfer rate between analyte (xanthine) and CH-TiO<sub>2</sub>/ITO electrode surface.  $XO_x$ /CH-TiO<sub>2</sub>/ITO electrode shows improved low response time 60 s, good sensitivity 0.577  $\mu$ A/mM, wider linear range 10 $\mu$ M – 250 $\mu$ M, and low detection limit 10 $\mu$ M for Xanthine. The fabricated electrode is also validated with the xanthine extracted from fresh catla fish samples. The results validate that CH-TiO<sub>2</sub>/ITO electrode can be used for other biosensors such as food freshness, detection of food toxins and other bioactive species.

## 5. REFERENCES

- [1] L Shen, L Yang, T Peng, “Amperometric determination of fish freshness by a hypoxanthine biosensor,”*J Sci Food Agr*, vol. 70, pp. 298–302, 1996.
- [2] AMulchandani, JHT Luong, KB Male, “Development and application of a biosensor for hypoxanthine in fish extract,”*Anal ChimActa*, vol.221, pp.215-22, 1989.
- [3] AKBasu, PChattopadhyaya, URoy Choudhury, “Development of an amperometric hypoxanthine biosensor for determination of hypoxanthine in fish and meat tissue,”*Indian J ExpBiol*, vol. 43, pp. 636-653, 2005.
- [4] P Pandey, M Datta, BD Malhotra, “Prospects of nanomaterials in biosensors”*Anal Lett*, vol. 41, pp. 159-209, 2008.
- [5] PR Solanki, A Kaushik, V Agrawal, BD Malhotra, “Nanostructured metal oxide based biosensors,”*Npg Asia Mater*, vol.3, pp. 17-24, 2011.
- [6] AT Lawal, SBAdelaju, “Polypyrrole-based xanthine oxidase potentiometric biosensor for hypoxanthine,”*J ApplSci*, vol. 8, pp. 2599-605, 2008.
- [7] JM Pingarrón, YS Paloma, GC Araceli, “Gold nanoparticle-based electrochemical biosensors,”*ElectrochimActa*, vol. 53, pp. 5848-66, 2008.
- [8] K Surendra, JSingh, VVAgrawal, BD Malhotra, “Nanostructured nickel oxide film for application to fish freshness biosensor,”*Applied Physics Letters*, vol. 101, 2012.
- [9] KK Rezaa, MK Singha, SKYadava, JSingh, Ved Varun Agrawala, B.D. Malhotrad, “Quantum dots based platform for application to fish freshness biosensor,”*Sensors and Actuators B*, vol. 177, pp. 627-633, 2013.

- [10] BD Malhotra, R Singhal, AChaubey, SK Sharma, A Kumar, "Recent Trends in Biosensors," *Current Applied Physics*, vol. 5, pp. 92-97, 2005.
- [11] SM Hudson, C Smith, "Polysaccharide: chitin and chitosan: chemistry and technology of their use as structural materials, Biopolymers from renewable resources," pp. 96-118, 1998.
- [12] MNV Ravikumar, PK Dutta, S Nakamura, "Chitosanamine oxide: a new gelling system, characterization and in vitro evaluations," *Indian J Pharma Sci*, vol. 55, 2000.
- [13] K Kurita, "Chemistry and application of chitin and chitosan," *Polym Degrad Stab*, vol. 59, 1998.
- [14] J Dutta, PK Dutta, "Tissue engineering: an emergent process for development of bio-products," *Industrial Products Finder*, vol. 246, 2003.
- [15] O Felt, P Buri, R Gurny, "Chitosan: a unique polysaccharide for drug delivery," *Drug Dev Ind Pharm*, vol. 24, pp. 979, 1998.
- [16] TR Sridhari, PK Dutta, "Synthesis and characterization of maleilated chitosan for dye house effluent," *Indian J Chem Tech*, vol. 7, pp. 198, 2000.
- [17] HY Dang, J Wang, SS Fan, "The synthesis of metal oxide nanowires by directly heating metal samples in appropriate oxygen atmospheres," *Nanotechnology*, vol. 14, pp. 738-741, 2003.

- [18] ZL Wang, "Functional oxide nanobelts: materials, properties and potential applications in nanosystems and biotechnology," *Annu. Rev. Phys. Chem.*, vol. 55, pp. 159-196, 2004.
- [19] JHuang, SViriji, BH Weiller, R BKaner, "Nanostructured polyaniline sensors," *Chem. Eur. J.*, vol. 10, pp. 1314-1319, 2004.
- [20] TVDinh, BM Cullum, DLStokes, "Nanosensors and biochips: frontiers in biomolecular diagnostics," *Sens. Act. B: Chem.*, vol. 74, pp. 2-11, 2001.
- [21] CJianrong, M Yuqing, H Nongyue, W Xiaohua, LSijiao, "Nanotechnology and biosensors," *Biotechnology Advances*, vol. 22, pp. 505-518, 2004.
- [22] ZL Wang, "Nanobelts, nanowires, and nanodiskettes of semiconducting oxides- from materials to nanodevices," *Adv. Mater.*, Vol. 15, pp. 432-436, 2003.
- [23] A Rothschild, Y Komem, "The effect of grain size on the sensitivity of nanocrystalline metal-oxide gas sensors," *J. Appl. Phys.*, vol. 95, pp. 6374, 2004.
- [24] LF Dong, ZL Cui, ZK Zhang, "Gas Sensing properties of nano-ZnO prepared by arc plasma method," *NanoStructured Mater.*, vol. 8, pp. 815-823, 1997.
- [25] N Yamazoe, G Sakai, K Shimano, "Oxide semiconductor gas sensors," *Catal. Surveys Asia*, vol. 1, pp. 63-75, 2003.
- [26] ZL Wang, "Nanostructures of zinc oxide," *Materialstoday*, vol. 7, pp. 26-33, 2004.



- [27] PM Chavhan, V Reddy, C Kim, "Nanostructured Titanium Oxide Platform for Application to Ascorbic Acid Detection," *Int J Electrochem Sci*, vol. 7, pp. 5420 – 5428, 2012.
- [28] S Dong, JXi, Y Wu, H Liu, C Fu, H Liu, FXiao, "High loading MnO<sub>2</sub> nanowires on graphene paper: Facile electrochemical synthesis and use as flexible electrode for tracking hydrogen peroxide secretion in live cells," *Analytica Chimica Acta*, vol. 853, pp. 200-206, 2015.
- [29] P. Judeinstein, C. Sanchez, "Hybrid organic–inorganic materials: a land of multidisciplinary," *J. Mater. Chem.*, vol. 6, pp. 511, 1996.
- [30] HS Nalwa, "Handbook of nanostructured materials and nanotechnology. New York: Academic press," 2000.
- [31] AS Edelstein, RC Cammarata, "Nanomaterials: synthesis, properties, and applications." Philadelphia, PA: Institute of Physics, 1996.
- [32] VM Shalaev, MMoskovits, "Nanostructured materials: clusters, composites, and thin films," *American Chemical Society*, 1997.
- [33] Y Xia, PYang, Y Sun, Y Wu, B Mayers, B Gates, Y Yin, F Kim, H Yan, "Onedimensional nanostructures: synthesis, characterization, and applications," *Adv. Mater.*, vol. 15, pp. 353-389, 2003.
- [34] AZ Sadek, SChoopun, W Wlodarski, SJIppolito, K.Kalantar-zadeh, "Characterization of ZnO nanobelt based gas sensor for H<sub>2</sub>, NO<sub>2</sub> and hydrocarbon sensing," *Sensors J.*, vol. 7, pp. 919-924, 2007.

- [35] XJ Huang, YK Choi, "Chemical sensors based on nanostructured materials," *Sens. Act. B: Chem.*, vol. 122, pp. 659-671, 2007.
- [36] CM Pandey, A. Sharma, G Sumana, ITiwari, BD Malhotra, "Cationic poly(lactic-co-glycolic acid) iron oxide microspheres for nucleic acid detection," *Nanoscale*, vol. 5, pp. 3800-3807, 2013.
- [37] A. Turner, IKarube,GS Wilson, "Biosensors: fundamentals and applications, " *Oxford university press*: 1987.
- [38] J Wang, "Nanomaterial-based electrochemical biosensors," *Analyst*, vol. 130, pp. 421-426, 2005.
- [39] XY Lang, HY Fu, C Hou, GF Han, P Yang, YB Liu, Q Jiang, "Nanoporous gold supported cobalt oxide microelectrodes as high-performance electrochemical biosensors," *Nature communications*, vol. 4, pp. 2169, 2013.
- [40] PR Solanki, A Kaushik, VV Agrawal, BD Malhotra, "Nanostructured metal oxide-based biosensors," *NPG Asia Mater*, vol. 3, pp. 17-24, 2011.
- [41] A Liu, "Towards development of chemosensors and biosensors with metal-oxide-based nanowires or nanotubes," *Biosensors and Bioelectronics*, vol. 24, pp. 167-177, 2008.
- [42] J Jiang, Y Li, X Huang, C Yuan, XWD Lou, "Recent advances in metal oxide-based electrode architecture design for electrochemical energy storage" *Advanced materials*, vol. 24, pp. 5166-5180, 2012.
- [43] J Hu, Y Qian, X Wang, TLiu, SLiu, "Drug-loaded and superparamagnetic iron oxide nanoparticle surface-embedded amphiphilic block copolymer micelles for integrated

chemotherapeutic drug delivery and MR imaging,"*Langmuir*, vol. 28, pp. 2073-2082, 2011.

[44] AE Nel, L Madler, D Velegol, T Xia, EMV Hoek, PSomasundaran, FKlaessig, V Castranova, M Thompson, "Understanding biophysicochemical interactions at the nano-bio interface,"*Nat Mater*, vol. 8, pp. 543-557, 2009.

[45] LBesra, MLiu, "A review on fundamentals and applications of electrophoretic deposition (EPD),"*Progress in Materials Science*, vol. 52, pp. 1-6, 2006.

[46] R Aldo, BJames, H.Dickerson, "Electrophoretic Deposition: Fundamentals and Applications,"*J. Phys. Chem. B*, vol. 117, pp. 1501-1507, 2013.

## **List of Publications**

- Ufana Riaz, S.M. Ashraf, **Vaibhav Budhiraja**, Sadaf Aleem and Jyoti Kashyap (2016) “*Comparative studies of the photocatalytic and microwave-assisted degradation of alizarin red using ZnO/poly (1-naphthylamine) nonohybrids.*” **Journal of Molecular liquids**, 216, 259-267. (I.F.- **4.513**)
- Ufana Riaz, S.M. Ashraf, Sadaf Aleem, **Vaibhav Budhiraja** and Sapana Jadoun (2016) “*Microwave-assisted green synthesis of some nanoconjugated copolymers: Characterisation and fluorescence quenching studies with bovine serum albumin.*” **New Journal of Chemistry**, 40 (5), 4643-4653. (I.F.- **3.201**)

Article published in **Rasayan 2018**, annual technical magazine, Department of Applied Chemistry, Delhi Technological University.

- **Vaibhav Budhiraja**, Chandra Mouli Pandey “*Nanostructured metal oxides based biosensor for enzyme detection.*”